Hittite Journal of Science and Engineering, 2023, 10 (1) 11-19
ISSN NUMBER: 2148-4171
DOI: 10.17350/HJSE19030000286

DFT Computations and Molecular Docking Studies of 3-(6-(3-aminophenyl)thiazolo[1,2,4]triazol-2-yl)-2H-chromen-2-one(ATTC) Molecule

Mehmet Baglan[1] **Kenan Goren**[1] **Umit Yildiko**[2]
[1]Kafkas University, Department of Chemistry, Kars, Turkey
[2]Kafkas University, Department of Bioengineering, Kars, Turkey

ABSTRACT

In this study, theoretic analyses were executed on the optimized geometric structure of 3-(6-(3-aminophenyl)thiazolo[3,2-b][1.2.4]triazol-2-yl)-2H-chromen-2-one (ATTC). The level of theory B3LYP/DGDZVP and B3LYP/6-311G(d,p) were used for these theoretical studies. To determine the stability and molecular reactiveness of the molecule, the energy range, the HOMO-LUMO energies, softhood (s), hardhood (η), electronic negativity (χ), and chemical potential (μ) characteristics were employed. The second array decay energy E(2) values of the molecule, which indicate the ATTC molecule's bioactivite, were determined with the native bond orbital (NBO) analysis. The ATTC molecule's reactive behavior is further studied using simulated molecular electrostatic potential (MEP) surface's calculations. The overall electron intensity and mulliken atomic charge distribution found by MEP area research gave proof that the molecule's reactive area existed. The ATTC molecule will continue to be a crucial therapeutic agent for Alzheimer disease's treatment Alzheimer disease thanks to a molecular docking study. The highest binding affinity was observed as a docking score of -10,681 kcal/mol.

Keywords:
CDFT calculation; FMO; NBO; Molecular docking

Article History:
Received: 2022/09/04
Accepted: 2022/12/29
Online: 2023/03/31

***Correspondence to**: Mehmet Baglan,*
Kafkas University, Department of Chemistry, 36100, Kars, Turkey.
E-Mail: mehmetbaglan@gmail.com
Phone: +90 (541) 538 14 82

INTRODUCTION

Triazoles are members of a family of five-membered heterocyclics that have received more attention than any other scientific field, largely due to their myriad uses in the disciplines of medicine, agriculture, and materials sciences fields.[1, 2], Among them, the 1,2,4-triazoles result from a precise arrangement of the three nitrogen atoms and the two carbon atoms, which confer unique properties combining different weak interactions, a characteristic basicity, and several coordination modes [3]. 1,2,4-Triazoles, antifungal [4], antibacterial [5], antioxidant [6], antitubercular [7], analgesic [8], anti-inflammatory [9], anticancer [10] or pesticide activities [11]. It is the cornerstone of many molecular structures exhibited. Triazoles are used in a wide variety of applications due to their capacity to add different substituents to all nitrogen and carbon atoms in the skeleton, which is vital for controlling these properties [12]. In this case, the scientific community has entered into a creative competition to create methods for forming triazoles with advantageous substituents.

Globally, older adults with Alzheimer's illness (AD) typically experience mind loss and behavioral changes [13]. This neurological condition, characterized by accelerated brain tissue degeneration, is caused by an acetylcholine (ACh) deficiency [14]. AChE and BChE enzymes are known as hydrolyze ACh in the human body [15]. Acetylcholine is broken down by AChE in the synaptic cleft of the brain [16]. Acetylcholine is therefore retained in the synaptic cleft for neurotransmission, thus minimizing or preventing the onset of AD symptoms [17]. Recent research has shown that loss of acetyltransferase activity and choline leads to a decrease in ACh as a neurotransmitter [18]. As an asymptomatic strategy, researchers have focused on cholinesterase (ChE) inhibition therapy [19]. According to reports, plant secondary metabolites exhibit ChE inhibitory properties that can be used to treat AD [20].

Recently, it has become common practice to use the density functional theory (DFT) approximation to reveal details about the electrical and geometric structure of molecules [21]. In recent studies, DFT in triazole derivatives has been the subject of molecular docking and vibration studies. We calculated the HOMO-LUMO gap, which affects stability, stiffness, and many other factors, using Frontier molecular orbitals (FMO), which are also determined using DFT simulations. To determine the maximum stabilization energy using the DFT method, NBO analysis was used to determine the electron density redistribution in antibonding orbitals energy differences and various bonding. The MEP surface image was taken and analyzed. Molecular docking experiments were analyzed to determine how the molecules interact with each other and to determine the target binding site of the ligand molecule. It was determined that the binding energy was the least. The literature search indicated that triazole derivatives may have commercial medical uses. Thus, the studied compound is coupled with AChE (7D9O) and BChE (7BO4).

MATERIALS AND METHODS

Ab initio and DFT techniques have come to the fore in recent years by making important developments in theoretical studies [22]. In particular, DFT methods based on Hartree-Fock (HF) methodologies yield results with great precision for structural elucidation of organic molecules. Therefore, in this study, the DFT technique was used to examine the ATTC molecule’s structural characteristics.

In order to do theoretical computations, the DFT/B3LYP/DGDZVP and DFT/B3LYP/6-311G(d,p) levels of theory were used with the Gaussian 09W [23] program. We studied and visualized the molecule’s structural characteristics with Gauss View 6.0.16. The ATTC molecule's geometries were optimized with DFT/B3LYP/DGDZVP and DFT/B3LYP/6-311G(d,p) level of theory. After optimization, harmonic frequency analysis is used to verify that the optimized geometries match the true global minimum, which is the equilibrium structure.

The binding affinity of the molecule (Maestro Molecular Modeling platform of the Schrödinger, LLC model (version 11.8)) was used to calculate the binding affinity. The crystal structures of acetylcholinesterase (AChE) protein (PDB ID: 7D9O) with a resolution factor of 2.45 Å and the crystal structure of butyrylcholinesterase (BChE) protein (PDB ID: 7BO4) with a resolution factor of 2.40 Å were resolved using the X-ray diffraction method. Retrieved from the PDB extension file and the RCSB Protein Data Bank (see https://www.rcsb.org/pdb). Ligand constructs were obtained as SDF files from the PubChem website. The compound was constructed using the Ligprep module in accordance with previous work. All the water molecules in the crystalline structure have been eliminated. By using this module to determine the protein’s active site for flexible binding, protein ion balance was improved. In accordance with previous studies, grid boxes were made by forming grids on the binding protein’s sites, using the receptor grid forming module to provide flexible clamping. The Glide docking module was used for ligand-protein docking research. Calculations were performed to identify ligands and enzymes with the highest binding affinities and conformations. The highest binding affinities are indicated by the lowest energy positions. Discovery Studio version 4.5 was used to visualize the resulting receptor 2D and 3D interactions (Visualizer 2005) (Fig 5 and 6).

RESULTS AND DISCUSSION

Bond Lengths and Bond Angles

The geometric parameters (bond angles (°) and bond lengths (Å)) computed with the B3LYP/DGDZVP and B3LYP/6-311G(d,p) level of theory were compared and it was seen that the two different parameters found were replicated very well [24, 25]. The geometry of composite ATTC, including bond lengths, twist angles, and bond angles, is presented in (Table 1). The bond length and the title structure's optimized geometry are as in Figures 1b and 1d). This title molecule has five C-H seven C - C, three different two (C - N, C - O and C - S) bond lengths and a single (N - N, C - H) bond length.

The maximum bond lengths to C12 and S11 were calculated and determined to be 1.76091 Å and 1.76109 Å, respectively (for B3LYP/DGDZVP and B3LYP/6-311G(d,p)). The computed bond length values to C - H and C - C in the benzene ring are between 1.39431 Å to 1.38827 Å and 1.41121Å -1.40669 Å with the B3LYP/DGDZVP and B3LYP/6-311G(d,p) level of theory and the C - C bond length, as well as C - H are between 1.08728 Å to 1.08425 Å and 1.08603 Å -1.08262 Å and the theoretical values are in strong agreement with each other. They found that there were some disparities at each stage of computing. Homonuclear bond lengths (N - N and C - C) are higher than heteronuclear bond lengths (N - H and C - H). The fact that opposite charges are attracted and the opposite charges are repellent is a significant factor.

Mulliken Atomic Charges

Mulliken charges are a result of Mulliken population analysis and offer a way to calculate partial atomic charges using computational chemistry methods [26, 27]. Mulliken atomic charge computing plays a significant role in applying quantum chemistry computing to molecular systems, as the molecular system’s atomic charges affect variables like reactivity, polarizability, and dipole moment [28, 29]. Using the B3LYP/DGDZVP and

Table 1. Theoretically obtained some bond lengths (Å), bond angles (°) and torsion angles (°) of the molecule.

Bond Lengths	**B3LYP/ DGDZVP**	**B3LYP / 6-311G(d,p)**	**Bond Lengths**	**B3LYP/ DGDZVP**	**B3LYP/6-311G(d,p)**
C1-C6	1.39431	1.38827	C10-N15	1.31989	1.31321
C3-C8	1.47343	1.46983	N9-N13	1.36032	1.35368
C8-C12	1.36587	1.36003	C12-S11	1.76091	1.76109
C14-C16	1.47234	1.46869	C10-S11	1.10990	1.73858
C16-C17	1.36287	1.35806	C1-H27	1.08728	1.08425
C16-C21	1.47594	1.47367	C12-H33	1.08074	1.07686
C18-C22	1.41121	1.40669	C17-H34	1.08745	1.08447
C19-O20	1.36581	1.35896	C25-H38	1.08603	1.08262
C21-O26	1.20796	1.19547	C22-H35	1.08773	1.08457
C5-N7	1.40448	1.39368	N7-H31	1.01378	1.00916
Bond Angles	**B3LYP/ DGDZVP**	**B3LYP /6-311G(d,p)**	**Bond Angles**	**B3LYP/DGDZVP**	**B3LYP/6-311G(d,p)**
C3-C2-C1	119.13896	119.07486	N15-C14-N13	115.72264	115.61049
C8-C3-C4	119.09447	119.04467	C4-C5-N7	120.57899	120.74727
C3-C8-C12	127.52849	127.54713	C19-O20-C21	123.42725	123.82507
C14-C15-C17	120.53946	120.46344	C5-N7-H32	114.60032	115.60223
C10-S11-C12	89.04246	89.02433	S11-C12-H33	119.18580	119.06605
Torsion Angles	**B3LYP/ DGDZVP**	**B3LYP /6-311G(d,p)**	**Torsion Angles**	**B3LYP/ DGDZVP**	**B3LYP/6-311G(d,p)**
C1-C2-C3-C8	177.52769	-177.45104	C4-C5-N7-H32	-27.81765	-24.02402
C16-C17-C18-C22	-179.83336	179.73873	N15-C10-S11-C12	178.80509	-178.72682
O26-C21-C15-C17	-173.81448	174.55803	C17-C16-C21-O26	-173.81448	174.55803

B3LYP/6-311G(d,p) level of theory, mulliken atomic charges for the molecule were calculated. The results were summarized in Table 2 and Fig. 1.

Table 2. Mulliken atomic charges computed by DFT/B3LYP/DGDZVP and DFT/B3LYP/6-311G(d,p) level of theory.

	B3LYP/ DGDZVP	**B3LYP/6-311G(d,p)**		**B3LYP/ DGDZVP**	**B3LYP/6-311G(d,p)**
C1	-0.213	-0.105	C23	-0.255	-0.096
C2	-0.361	-0.039	C24	-0.210	-0.081
C3	0.240	-0.083	C25	-0.351	-0.072
C4	-0.453	-0.048	O20	-0.313	-0.318
C5	0.375	0.101	O26	-0.306	-0.273
C6	-0.355	-0.067	N7	-0.766	-0.471
C8	0.317	0.356	N9	-0.039	-0.335
C10	0.014	0.176	N13	-0.275	-0.238
C12	-0.548	-0.389	N15	-0.223	-0.308
C14	0.206	0.243	S11	0.223	0.287
C16	-0.060	-0.295	H31	0.347	0.208
C17	0.297	0.151	H32	0.345	0.206
C18	0.210	-0.174	H34	0.265	0.114
C19	0.316	0.226	H35	0.231	0.096
C21	0.335	0.423	H36	0.230	0.100
C22	-0.328	-0.048	H37	0.232	0.104

It was discovered that molecular relaxation causes all nitrogen and oxygen to compute a negative charge. However, despite having varying charges, all hydrogen atoms show a net positive charge. In the B3LYP/DGDZVP and B3LYP/6-311G(d,p) level of theory, C5, C8, C10, C14, C17, C19 and C21 atoms show positive charges, while all remaining carbon atoms exhibit negative charges. These findings made it clear that these atoms were the places most responsive to the reaction. Due to the O atom's substantial negative charge and the H atom's net positive charge, a type of solid intermolecular interaction may have taken place.

Figure 1. ATTC molecule with DFT/B3LYP/6-311G(d,p) basis set a) mulliken b) bond length c) atomic mass d) structure optimization

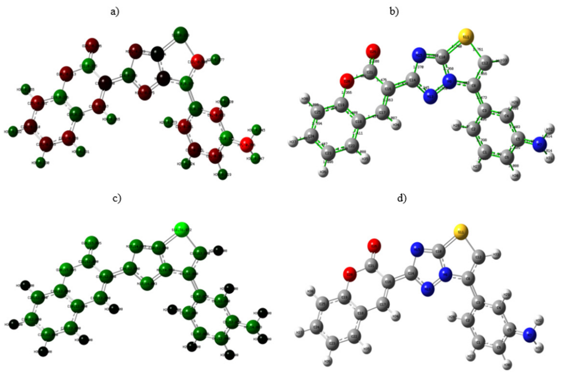

NLO-Nonlinear Optical Properties

Research in signal processing, optical interconnects, and telecommunications to develop nonlinear optical materials is a remarkable area [30, 31]. The NLO properties of a molecule are the result of electromagnetic fields that phase change and the frequency of electromagnetic waves when interacting with different media [32]. The hyperpolarizability (β) and polarizability (α) values associated with a molecule can be used to predict NLO attributes [33]. DFT-based simulations can efficiently predict a molecule's potential for use as a nonlinear optical compound [34].

Theoretically, the NLO properties of a molecule are based on its initial hyperpolarizability (β_0). To compare NLO properties on two different basis sets, it is used to say that chemical systems with higher first-order hyperpolarizability (β_0) have higher NLO properties [35]. The Gaussian log file used in the DFT calculation was used to derive the hyperpolarizability tensors of ATTC (βxxy, βxxx, βxyy, βxxz, βyyy, βxyz, βyyz, βyzz, βxzz, βzzz). The first-order hyperpolarizability (β_0) values for ATTC calculated with the DFT/B3LYP/DGDZVP and B3LYP/6-311G(d,p) level of theory are 2.718×10^{-30} esu and 2.606×10^{-30} esu and are given in Table 3.

$$\beta o = [(\beta xxx + \beta xyy + \beta xzz)^2 + (\beta yyy + \beta yxx + yzz)^2 + ((\beta zzz + \beta zxx + \beta zyy)^2]^{1/2} \quad (1)$$

Table 3. DFT/B3LYP- B3LYP belong to DGDZVP and 6-311G(d,p) basis set calculated dipole moments (Debye), (au) polarizability, β components, and β tot PEP value.

Parameters	B3LYP/ DGDZVP	B3LYP/ 6-311G(d,p)	Parameters	B3LYP/ DGDZVP	B3LYP/ 6-311G(d,p)
μ x	5.0088	4.3499	β XXX	166.1076	41.7410
μ y	-5.2530	-5.7790	β XXY	-108.2733	-116.5261
μ z	1.3968	-2.8418	β XYY	53.5541	76.0196
μ (D)	7.3914	7.7714	β YYY	-58.6642	-70.2596
α xx	-103.0413	-116.7994	β XXZ	20.3758	-97.2282
α zz	-161.9383	-156.6253	β YYZ	5.4879	-18.0898
α yy	-155.4204	-151.0134	β XYZ	25.5723	11.6749
α XY	17.1890	11.9881	β XZZ	-3.7551	19.0652
α YZ	6.5478	-0.9616	B ZZZ	-7.6785	1.5972
α XZ	-5.1234	-7.3691	β YZZ	2.8195	-3.7277
α (au)	-140.1334	-141.4793	B0 (esu)	2.718×10^{-30}	2.606×10^{-30}

Frontier Molecular Orbital (FMO) Analysis

Frontier molecular orbitals (FMO) are defined as the lowest unoccupied molecular orbital (LUMO) and the highest occupied molecular orbital (HOMO) [36]. The research of a compound's electrical, optical, and chemical properties benefits tremendously from the use of FMOs [37]. In addition, it predicts a number of conjugated system reactions, as well as its positioning in the most reactive π-electron system. HOMO shows a number of significant donor orbitals, while LUMO shows prominent acceptor orbitals [38].

Green and red colors are represented the HOMO and LUMO orbitals, respectively [38]. The former denotes negatively charged surfaces or electrophiles, while the latter represents positively charged surfaces or nucleophiles. The charge transfer interaction that occurs within the molecule may be seen in the HOMO-LUMO energy gap [39]. Electronic absorption occurs when an electron is exhipped from the highest occupied molecular orbital (HOMO) to the lowest unoccupied molecular orbital (LUMO) during the transition from the ground state to the first excited state [40].

Orbital energy level analyses to ATTC material using DFT/B3LYP/DGDZVP and DFT/B3LYP/6-311G(d,p) level of theory, EHOMO value in the first method -6.0762 eV, ELUMO value -2.2715 eV and ΔE 3.8047 eV in the second method, EHOMO value in the second method It was found that -5.9752 eV, ELUMO value -2.17 eV and ΔE value of 3.8052 eV. Theoretical energy band gap values produced from FMOs differ when both values are made comparison. In terms of LUMO and HOMO orbital energies, the electron affinity and ionization energy are symbolized by A = -ELUMO and I = -EHOMO, respectively.

While the electronegativity (χ) is defined as (I + A)/2, the calculated electro-negativity (χ) of the ATTC molecule in the first method is 1.6357 eV, and in the second method, the electro-negativity (χ)) is 1.5850 eV. In Figs. 2 and 3, the border molecular orbitals (HOMO and LUMO) are displayed at the B3LYP/DGDZVP and the B3LYP/6-311G(d,p) level of theory, respectively.

Molecular Electrostatic Potential (MEP) Maps

The molecular electrostatic potential (MEP) is a method used to investigate the molecular characteristics of tiny molecules, the activities of pharmacological compounds and their analogs, the biological role of hemoglobin, and the catalytic activity of enzymes. It offers a visual way to comprehend the molecule's relative polarity. Electrosta-

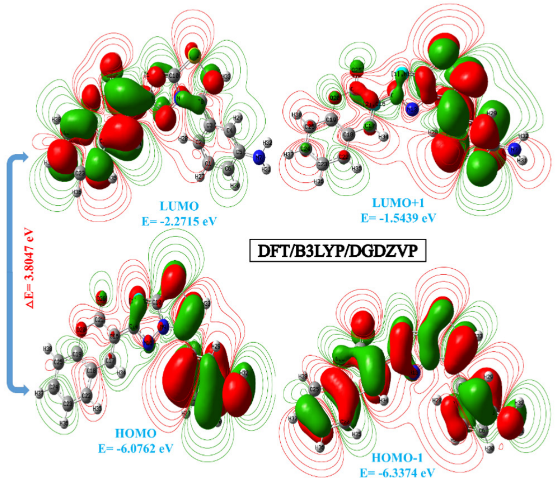

Figure 2. Boundary molecular orbitals of the ATTC compound relative to the DFT/B3LYP/DGDZVP level

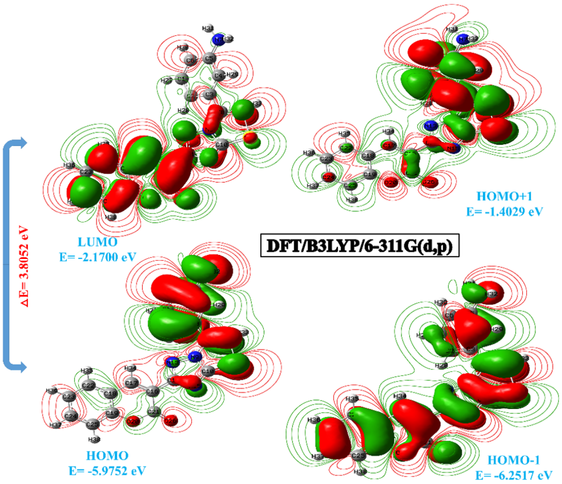

Figure 3. Boundary molecular orbitals of the ATTC compound according to the DFT/B3LYP/6-311G(d,p) level

tic potential surface density and the chemical reactivity site of the molecules are mapped on an electron density isosurface. With the level of theory B3LYP/DGDZVP and B3LYP/6311G(d,p), MEP was computed in DFT mode. As a result, many hues were seen, each of which represented a unique electrostatic potential [41, 42]. Fig. 4 depicts the colored MEP surface map. The electrostatic potential rises in the yellow, orange, blue, and green directions. A positive area close to the hydrogen atoms (31H-32H) that are colored blue is more likely to be attacked by a nucleophile. The color green denoted the absence of potential. The oxygen atom in the compound ATTC, which is electronegative, is in the negative field, which is represented by the color red. The negative and positive poles of the compound's electrostatic potential, respectively, serve as indicators of its electrophile and nucleophile appeal.

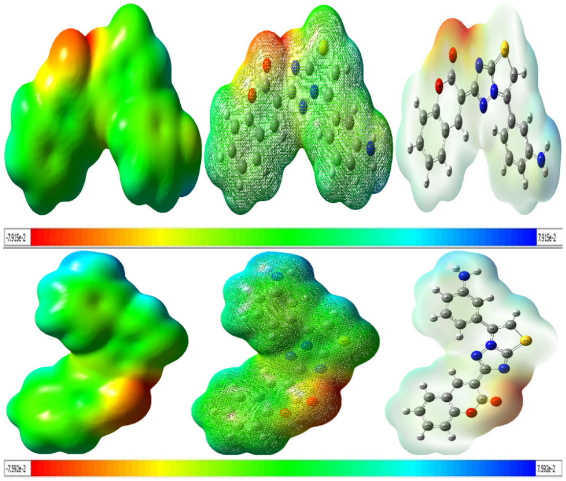

Figure 4. Molecular electrostatic potential surface by DFT/B3LYP and DFT/B3LYP methods with DGDZVP and 6-311G(d,p) basis set

Natural Bond Orbital (NBO) Analysis

At the DFT/B3LYP/DGDZVP and DFT/B3LYP/6-311G(d,p) level of theory, delocalization of the electron density between occupied Lewis type (bond or lone pair)

Table 4. Calculated quantum chemical parameters*(in eV) for low energy compatibilities by DFT/B3LYP/DGDZVP-DFT/B3LYP/6-311G(d,p) level of theory of the ATTC molecule.

Molecules Energy		DFT/ B3LYP/ DGDZVP	DFT/B3LYP/ 6-311G(d,p)
ELUMO		-2.27157	-2.17007
EHOMO		-6.07621	-5.97526
ELUMO+1		-1.54395	-1.4029
EHOMO-1		-6.33744	-6.2517
Energy Gap	(Δ)|EHOMO- ELUMO|	3.80464	3.80519
Electron Affinity	(A = –ELUMO)	2.27157	2.1700
Ionization Potential	(I = –EHOMO)	6.07621	5.97526
Chemical hardness	(η = (I – A)/2)	1.9023	1.90259
Chemical softness	(s = 1/2 η)	0.95116	0.95129
Electronegativity	(χ =(1+ A)/2)	1.6357	1.5850
Chemical Potential	(μ =–(I + A)/2)	-4.17	-4.07
Electrophilicity index	(ω= μ2/2 η)	4.57049	4.35325

NBO orbitals and formally unoccupied (anti-bond or Rydberg) non-Lewis NBO orbitals corresponding to a stabilizing donor–acceptor interaction was carried out. It is possible to look at a molecule's hyperconjugative interactions by utilizing information from NBO analyses [43, 44]. When these interactions include moving electron density from the donor orbital to the acceptor orbital, the system stabilizes. Molecular interactions' magnitude and the stabilization energy are strongly correlated; the more interactions there are, the more energy there is in those interactions.

A complete NBO and quadratic Fock matrix perturbation theory study for ATTC was conducted to look into the intermolecular interaction. Table 5 lists the notable hyperconjugative interactions found in ATTC. Large E(2) values in NBO analyses indicate a greater system-wide degree of conjugation as well as active interactivity between electron acceptors and electron donors. The interactivities of the (σ/π) bond and the (σ*/π*) anti-bond also contributed significantly to the structure's stability, with the π(C18-C19) /π*(C16-N17) interaction having the highest E(2), followed by π(C8-C12) /π*(C2-C3) with 57.60 kcal/mol. Afterwards, we observed that the σ (C14-N15)/σ* (C10-S11) interaction also had the highest E(2) value with 11.46 kcal/mol.

Molecular Docking Studies

Molecular docking is a technique used to study the ligand-receptor binding mechanism and to understand the molecular interactions between binding modes [45, 46]. Selected binding sites of the receptor and ligands were determined using molecular insertion, which also serves to essentially confirm the results of the experiment. Two good docking scores were found in this study, which consisted of one compound and two enzyme sets (Tab-

Table 5. CSelected NBO results for ATTC utilizing the B3LYP/6-311G(d,p) theory level to show the generation of Lewis and non-Lewis orbitals.

NBO(i)	Type	ED/e	NBO(j)	Type	ED//e	E(2)[a] (Kcal/mol)	E (j)-E(i)[b] (a.u.)	F (i, j)[c] (a.u)
C1-C6	Π	1.69990	C2-C3	π*	0.39812	17.22	0.29	0.064
C1-C2	σ	1.97626	C3-C8	σ*	0.03435	4.08	1.16	0.061
C1-C6	π	1.69990	C4-C5	π*	0.39239	22.45	0.28	0.073
C2-C3	π	1.65267	C1-C6	π*	0.33804	22.78	0.28	0.072
C1-H27	σ	1.97812	C2-C3	σ*	0.02464	4.10	1.08	0.059
C2-C3	σ	1.65267	C3-C4	σ*	0.02211	4.73	1.25	0.069
C2-C3	π	1.65267	C8-C12	π*	0.28698	16.69	0.25	0.059
C2-H28	σ	1.97766	C3-C4	σ*	0.02211	4.64	1.07	0.063
C3-C8	σ	1.96405	C8-C12	σ*	0.02063	6.21	1.24	0.079
C4-C5	σ	1.97057	C3-C4	σ*	0.02211	4.03	1.26	0.064
C4-C5	π	1.64441	C1-C6	π*	0.33804	16.47	0.29	0.062
C4-C5	π	1.64441	C2-C3	π*	0.39812	23.23	0.29	0.074
C4-H29	σ	1.97845	C2-C3	σ*	0.02464	4.32	1.09	0.061
C5-C6	σ	1.97168	C4-C5	σ*	0.02328	4.27	1.26	0.066
C6-H30	σ	1.97870	C4-C5	σ*	0.02328	4.26	1.08	0.061
N7-H32	σ	1.98801	C5-C6	σ*	0.02489	4.06	1.20	0.063
C10-N15	π	1.81178	N13-C14	π*	0.42126	31.13	0.32	0.094
C16-C17	π	1.78974	C21-O26	π*	0.25662	21.77	0.30	0.073
C8-C12	σ	1.89837	N9-N13	σ*	0.02527	5.90	1.13	0.073
C14-N15	σ	1.96841	C10-S11	σ*	0.04060	11.46	0.97	0.094
C18-C19	π	1.58588	C22-C23	π*	0.30021	19.54	0.29	0.070
C22-C23	π	1.70010	C24-C25	π*	0.31366	21.07	0.29	0.070
C24-C25	π	1.68445	C18-C19	π*	0.43452	22.75	0.28	0.073
C8-C12	π	1.89837	C2-C3	π*	0.39812	57.60	0.03	0.063
N13-C14	π	1.86953	C16-C17	π*	0.17883	40.71	0.04	0.062
C18-C19	π	1.58588	C16-C17	π*	0.17883	155.91	0.01	0.075
O20-C21	σ	1.99004	C19-O20	σ*	0.03438	11.10	0.06	0.078
C24-C25	π	1.68445	C22-C23	π*	0.30021	17.59	0.29	0.064

[a] The energy of a hyper conjugative interaction is denoted by E (2). (stabilization energy).

[b] The energy disparity between the acceptor and donor NBO orbitals.

[c] The Fock matrix element between the i and j NBO orbitals is called F(i, j).

le 6). The results of the coupling of these ligands to the enzyme's catalytic active site were evaluated in terms of binding affinity and interaction pattern. The BChE enzyme has the highest binding affinity score in terms of molecular structure. Since it is structural, the similarity between the protein and the natural ligand increases this value.

Table 6. Docking score of ATTC - AChE and ATTC - BChE

Compound	Docking Score	
	AChE (PDB: 7D9O)	BChE (PDB: 7BO4)
ATTC	-10.124 kcal/mol	-10.681 kcal/mol

The dynamics of the proteins is a key factor when proteins interact with various derivatives to produce complexes that can improve or impair their biological functions. The binding modes were examined to understand the inhibitory mechanisms after the best exposure was selected in the entire ligand-enzyme insertion study. The results of the ATTC -AChE insertion probe are shown in Fig. 5 as 3D and 2D interactions. The binding affinity with ATTC -AChE resulted in the calculation of the affinity score of -10.124 kcal/mol. It has been determined in Table 7 that many interactions, such as Conventional Hydrogen Bonding, Pi-Sulfur, Pi-Pi T-Shapeding, Pi-Pi Stacking in the binding site with ATTC-AChE.

Table 7. Docking results on the binding site of the ATTC molecule with the AChE protein.

Enzyme	Interaction Type	Amino Acid	Bond Length
AChE	Conventional Hydrogen Bond	PHE-295	5.54 Å
	Carbon Hydrogen Bond	TYR-72	5.66 Å
		GLY-120	3.30 Å
		SER-293	4.06-4.63 Å
	Halogen (Fluorine)	GLU-202	4.63 Å
	π -Cation	TYR-337	5.13 Å
		ASP-74	7.43Å
	π -Sigma	TYR-337	3.30 Å
	π - π Stacked	TRP-86	3.80 Å
		TRP-286	5.99 Å
		TYR-341	4.31 Å
	π -Alkyl	TRP-286	4.38 Å
		TYR-72	5.35 Å

The results of the ATTC-BChE insertion probe are shown in Fig. 6 as 3D and 2D interactions. The binding affinity with ATTC-BChE resulted in the calculation of the affinity score of -10,681 kcal/mol. It has been determined in Table 8 that many interactions, such as Conventional Hydrogen Bonding, Pi-Pi T-Shapeding, Pi-Pi Stacking, Amide–Pi T- Stacking, Pi-Alkly in the binding site with ATTC-BChE.

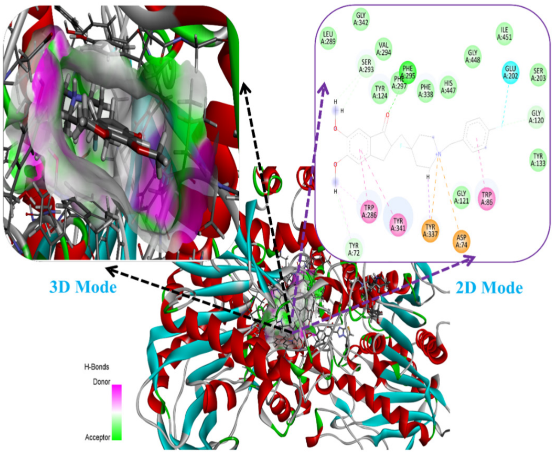

Figure 5. 3D representation of the receptor's aromatic surface and a 2D image of the ATTC-AChE enzyme contacts

Table 8. Results of insertion on the binding site with the ATTC-BChE protein.

Enzyme	Interaction Type	Amino Acid	Bond Length
BChE	Conventional Hydrogen Bond	ASN-256	4.57 Å

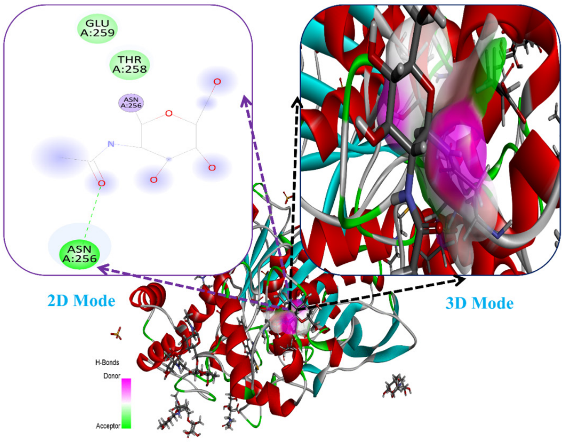

Figure 6. 3D representation of the receptor's aromatic surface and a 2D image of the ATTC-BChE enzyme contacts.

CONCLUSION

In this study, quantum chemical computations were used to conduct theoretical research on the ATTC molecule. Using the DFT-B3LPY/DGDZVP and 6-311G(d,p) level of theory, the compound's structural, frequency, electronic, and vibrational components were computed. Bond lengths, dihedral angles, and bond angles were discovered as structural characteristics. It was determined that the examined compound might be employed NLO material after looking at its nonlinear optical characteristics. Because the calculations for the ATTC molecule allowed the parameters of polarity (α = -140.1334 au and α = -141.4793 au) and static high-order polarity (β = 2.718 x 10^{-30} esu and β = 2.606 x 10^{-30} esu) to be determined. A strong candidate for nonlinear optical materials was considered to have potentially high polarity values from the data collected for the ATTC molecule. Mulliken payloads, HOMO-LUMO and MEP maps are also displayed. Consequently, compounds' docking studies, receptor compounds were investigated, and it was discovered that BChE was very efficient by its receptor shift point. Following such extensive pharmacological and clinical testing, these novel enzyme inhibitors may be taken into account for developing new AD medication formulations.

CONFLICT OF INTEREST

The article authors declare that there is no conflict of interest between them

AUTHOR CONTRIBUTION

The authors declare that they have contributed equally to the article.

REFERENCES

1. Kotian, S.Y., et al., Small molecule based five-membered heterocycles: A view of liquid crystalline properties beyond the biological applications. Journal of Molecular Liquids, 2020. 297: p. 111686.
2. Lohith, T.N., et al., Synthesis, molecular structure, Hirshfeld surface, energy framework and DFT studies of 1,3,4 oxadiazole derivative. Journal of Molecular Structure, 2022. 1252: p. 132203.
3. Ding, J., et al., One-step fabrication of nitrogen-deficient carbon nitride through pyrolysis of melamine and 1,2,4-triazole for its enhanced photocatalytic degradation. Green Chemical Engineering, 2021. 2(3): p. 317-326.
4. Sanina, N.A., et al., Synthesis, structure and antibacterial activity of dinitrosyl iron complexes (DNICs) dimers functionalized with 5-(nitrophenyl) -4-H-1,2,4-triazole-3-thiolyls. Polyhedron, 2022. 220: p. 115822.
5. Sadeghian, S., et al., 1,2,4-Triazole derivatives as novel and potent antifungal agents: Design, synthesis and biological evaluation. Journal of Molecular Structure, 2023. 1271: p. 134039.
6. Suresh Kumar, G.V., et al., Synthesis of some novel 2-substituted-5-[isopropylthiazole] clubbed 1,2,4-triazole and 1,3,4-oxadiazoles as potential antimicrobial and antitubercular agents. European journal of medicinal chemistry, 2010. 45(5): p. 2063-74.
7. Lao, Y., et al., Discovery of 1,2,4-triazole derivatives as novel neuroprotectants against cerebral ischemic injury by activating antioxidant response element. Bioorganic Chemistry, 2022. 128: p. 106096.
8. Grytsai, O., et al., Synthesis and biological evaluation of 3-amino-1,2,4-triazole derivatives as potential anticancer compounds. Bioorg Chem, 2020. 104: p. 104271.
9. Abdelazeem, A.H., et al., Design, synthesis and anti-inflammatory/analgesic evaluation of novel di-substituted urea derivatives bearing diaryl-1,2,4-triazole with dual COX-2/sEH inhibitory activities. Journal of Molecular Structure, 2021. 1240: p. 130565.
10. Martínez-Escudero, C.M., et al., Remediation of triazole, anilinopyrimidine, strobilurin and neonicotinoid pesticides in polluted soil using ozonation and solarization. Journal of Environmental Management, 2022. 310: p. 114781.
11. Abdelli, A., et al., Recent advances in the chemistry of 1,2,4-triazoles: Synthesis, reactivity and biological activities. Tetrahedron Letters, 2021. 86: p. 153518.
12. Minto-García, A., et al., Lexical relations in Spanish-Speaking older adults with Alzheimer's disease: An approach to semantic memory. Journal of Neurolinguistics, 2022. 62: p. 101059.
13. Mustafa, I.H., et al., Effect of cholineacetyltransferase activity and choline recycle ratio on diffusion-reaction modeling, bifurcation and chaotic behavior of acetylcholine neurocycle and their relation to Alzheimer's and Parkinson's diseases. Chemical Engineering Science, 2012. 68(1): p. 19-35.
14. Gao, H., et al., Pharmacophore-based drug design of AChE and BChE dual inhibitors as potential anti-Alzheimer's disease agents. Bioorg Chem, 2021. 114: p. 105149.
15. Aidoo, A.Y. and K. Ward, Spatio-temporal concentration of acetylcholine in vertebrate synaptic cleft. Mathematical and Computer Modelling, 2006. 44(9): p. 952-962.
16. Ahmad, W., Glucose enrichment impair neurotransmission and induce Aβ oligomerization that cannot be reversed by manipulating O-β-GlcNAcylation in the C. elegans model of Alzheimer's disease. The Journal of Nutritional Biochemistry, 2022. 108: p. 109100.
17. Liu, J., et al., Choline acetyltransferase and vesicular acetylcholine transporter are required for metamorphosis, reproduction, and insecticide susceptibility in Tribolium castaneum. Gene, 2022. 842: p. 146794.
18. Marucci, G., et al., Efficacy of acetylcholinesterase inhibitors in Alzheimer's disease. Neuropharmacology, 2021. 190: p. 108352.
19. Dos Santos, R., et al., Acetylcholinesterase and butyrylcholinesterase inhibition by nectriapyrone and tryptophol isolated from endophytic fungus Phomopsis sp. Nat Prod Res, 2022. 36(16): p. 4153-4158.
20. Ahmed Sameer, K. and T. Mohammed Hussein, Study geometrical, electronic and spectroscopic properties of BeO wurtzoids via DFT. Materials Today: Proceedings, 2021. 42: p. 2629-2637.
21. Sharma, D. and S. Nath Tiwari, Molecular Structure and Vibrational Dynamics Studies of 4-n-propyl-4′-cyanobiphenyl using Ab initio and DFT Methods. Materials Today: Proceedings, 2018. 5(7, Part 2): p. 15325-15334.
22. Deepa, H.R., S. Chandrasekhar, and J. Thipperudrappa, Investigation of FRET from organic dyes to silver nanoparticles and structural properties using the DFT/TD-DFT approach. Chemical Physics Impact, 2022. 4: p. 100075.
23. Frisch, M.J. and e. al, Gaussian 09, . Revision E.01.
24. Hernández, J.G., et al., Understanding of [RuL(ONO)](n+) acting as nitric oxide precursor, a theoretical study of ruthenium complexes of 1,4,8,11-tetraazacyclo- tetradecane having different substituents: How spin multiplicity influences bond angle and bond lengths (Ru-O-NO) in releasing of NO. J Inorg Biochem, 2021. 218: p. 111406.
25. Southern, S.A. and D.L. Bryce, To what extent do bond length and angle govern the ^{13}C and ^{1}H NMR response to weak CH···O hydrogen bonds? A case study of caffeine and theophylline cocrystals. Solid State Nuclear Magnetic Resonance, 2022. 119: p. 101795.
26. Yildiko, U., et al., Investigation of novel diethanolamine dithiocarbamate agent for RAFT polymerization: DFT computational study of the oligomer molecules. Bulletin of Materials Science, 2021. 44.
27. Satheeshkumar, R., et al., Spectroscopic (FT-IR, NMR, single crystal XRD) and DFT studies including FMO, Mulliken charges, and Hirshfeld surface analysis, molecular docking and ADME analyses of 2-amino-4′-fluorobenzophenone (FAB). Journal of Molecular Structure, 2022. 1267: p. 133552.
28. Krishna Kumar, V., et al., Vibrational assignment of the spectral data,

molecular dipole moment, polarizability, first hyperpolarizability, HOMO–LUMO and thermodynamic properties of 5-nitoindan using DFT quantum chemical calculations. Spectrochimica Acta Part A: Molecular and Biomolecular Spectroscopy, 2014. 118: p. 663-671.

29. Oftadeh, M., S. Naseh, and M. Hamadanian, Electronic properties and dipole polarizability of thiophene and thiophenol derivatives via density functional theory. Computational and Theoretical Chemistry, 2011. 966(1): p. 20-25.
30. Yahya, M., G. Kurtay, and A. Suvitha, On the Viability of Divergent Donor Moieties in Malononitrile-Based Donor-π-Acceptor NLO active materials: A DFT/TD-DFT Study. Journal of Physical Organic Chemistry, 2022. 35.
31. Rashid, M., et al., Nonlinear optical (NLO) response of boron phosphide nanosheet by alkali metals doping: A DFT study. Materials Science in Semiconductor Processing, 2022. 151: p. 107007.
32. Bi, Z., et al., Experimental and theoretical study on broadband electromagnetic wave absorption of algae-like NiO/carbon nanotubes absorbers. Journal of Alloys and Compounds, 2022. 926: p. 166821.
33. Jothi, A.I., M.W.B. Paul, and V. Alexander, A comparative molecular structure – NLO activity study of ortho-bridged dibenzaldehydes: Synthesis, crystal structure, SHG, and DFT studies. Journal of Molecular Structure, 2022. 1250: p. 131776.
34. Derafa, W., et al., An unexpected single crystal structure of nickel(II) complex: Spectral, DFT, NLO, magnetic and molecular docking studies. Journal of Molecular Structure, 2022. 1264: p. 133190.
35. Slyvka, Y., et al., Crystal structure, DFT-study and NLO properties of the novel copper(I) nitrate π,σ-coordination compound based on 1-allyl-3-norbornan-thiourea. Polyhedron, 2022. 211: p. 115545.
36. Yildiko, U., et al., Computational DFT calculations, photovoltaic properties and synthesis of (2R, 3S)-2, 3, 4-trihydroxybutoxy substituted phthalocyanines. Inorganic and Nano-Metal Chemistry, 2020. 50.
37. Buvaneswari, M., et al., Synthesis, growth, structural, spectroscopic, optical, thermal, DFT, HOMO–LUMO, MEP, NBO analysis and thermodynamic properties of vanillin isonicotinic hydrazide single crystal. Journal of Molecular Structure, 2021. 1243: p. 130856.
38. Sowrirajan, S., et al., (E)-4-((4-Bromobenzylidene) Amino)-N-(Pyrimidin-2-yl) Benzenesulfonamide from 4-Bromobenzaldehyde and Sulfadiazine, Synthesis, Spectral (FTIR, UV–Vis), Computational (DFT, HOMO–LUMO, MEP, NBO, NPA, ELF, LOL, RDG) and Molecular Docking Studies. Polycyclic Aromatic Compounds, 2022.
39. Sakr, M.A.S. and M.A. Saad, Spectroscopic investigation, DFT, NBO and TD-DFT calculation for porphyrin (PP) and porphyrin-based materials (PPBMs). Journal of Molecular Structure, 2022. 1258: p. 132699.
40. Aboalhassan, A.A., et al., 1,4-bis[β-(2-benzoxazoly1) vinyl] benzene (BBVB) laser dye and sodium salt of meso-tetrakis (4-sulfonatophenyl) porphyrin (TPPS); spectroscopic investigation and DFT, NBO and TD-DFT calculations. Journal of Photochemistry and Photobiology A: Chemistry, 2022. 431: p. 114039.
41. Singh, P., et al., Spectroscopic investigation (FT-IR, FT-Raman), HOMO-LUMO, NBO, and molecular docking analysis of N-ethyl-N-nitrosourea, a potential anticancer agent. Journal of Molecular Structure, 2018. 1154: p. 39-50.
42. Balachandran, V., et al., Conformational stability, spectroscopic and computational studies, HOMO–LUMO, NBO, ESP analysis, thermodynamic parameters of natural bioactive compound with anticancer potential of 2-(hydroxymethyl)anthraquinone. Spectrochimica Acta Part A: Molecular and Biomolecular Spectroscopy, 2015. 150: p. 631-640.
43. Balachandran, V. and V. Karpagam, Conformational stability, vibrational assignments of 2,3-dihydroxy benzaldehyde as supported by ab initio, hybrid density functional theory and normal coordinate analysis. Journal of Molecular Structure, 2013. 1038: p. 52-61.
44. Rezkallah, E., et al., DFT and Thermal Decomposition Studies on Gemcitabine. 2019. 233(10): p. 1503-1527.
45. Celik, S., S. Akyuz, and A.E. Ozel, Vibrational spectroscopic characterization and structural investigations of Cepharanthine, a natural alkaloid. Journal of Molecular Structure, 2022. 1258: p. 132693.
46. Celik, S., S. Akyuz, and A.E. Ozel, Molecular modeling, DFT quantum chemical analysis, and molecular docking on edotecarin, an indolocarbazole anticancer agent. Molecular Crystals and Liquid Crystals, 2022: p. 1-23.